



1 **Modeled source apportionment of black carbon particles coated with a light-scattering shell**

2

3

Aki Virkkula

4

Finnish Meteorological Institute

5

Helsinki, Finland

6

7 **Abstract**

8 The Aethalometer model has been used widely for estimating the contributions of fossil fuel emissions
9 and biomass burning to equivalent black carbon (eBC). The calculation is based on measured absorption
10 Ångström exponents (α_{abs}). The interpretation of α_{abs} is ambiguous since it is well-known that it not
11 only depends on the dominant absorber but also on the size and internal structure of the particles, core
12 size and shell thickness. In this work the uncertainties of the Aethalometer-model-derived apparent
13 fractions of absorption by eBC from fossil fuel and biomass burning are evaluated with a core-shell Mie
14 model. Biomass-burning fractions (BB(%)) were calculated for pure and coated single BC particles, for
15 lognormal unimodal and bimodal size distributions of BC cores coated with ammonium sulfate, a
16 scattering-only material. BB(%) was very seldom 0% even though BC was the only absorbing material in
17 the simulations. The shape of size distribution plays an important role. Narrow size distributions result
18 in higher α_{abs} and BB(%) values than wide size distributions. The sensitivity of α_{abs} and BB(%) to
19 variations in shell volume fractions is the highest for accumulation mode particles. This is important
20 because that is where the largest aerosol mass is. For the interpretation of absorption Ångström
21 exponents it would be very good to measure BC size distributions and shell thicknesses together with
22 the wavelength dependency of absorption.

23

24 **1. Introduction**

25 Incomplete combustion of organic fuels results in emission of light-absorbing carbon (LAC) particles
26 that contain both black carbon (BC) and brown carbon (BrC). BrC is light-absorbing organic matter in
27 atmospheric aerosols of various origins e.g., soil humics, humic-like substances (HULIS), tarry materials
28 from combustion, bioaerosols (Andreae and Gelencser, 2006; Laskin et al., 2015). BrC can significantly
29 absorb solar radiation in the ultraviolet–visible (uv–vis) wavelength range ($\lambda \approx 300 - 800$ nm). The



1 radiative effects of BC and BrC vary in time during atmospheric aging. For many combustion sources
2 the absorbance in fresh emission is almost completely caused by BC particles but during atmospheric
3 transport they often get coated with some light-scattering compounds, for instance ammonium sulfate
4 or light-absorbing organic carbon, BrC. For some sources (e.g. biomass burning) BrC may contribute
5 substantially to light-absorption already in the directly emitted aerosols and either increase or decrease
6 during aging. Thus, BrC is highly time-dependent as it's composition and absorption properties change
7 during atmospheric oxidation processes (Laskin et al., 2015).

8

9 The absorption coefficient σ_{ap} is approximately proportional to the power function $\lambda^{-\alpha_{abs}}$ where λ is
10 the wavelength and α_{abs} is the absorption Ångström exponent. α_{abs} is generally used to distinguish
11 aerosol types: for pure BC particles $\alpha_{abs} \approx 1$ while other light absorbing aerosols (BrC, soil dust) it is
12 clearly > 1 (e.g., Kirchstetter et al., 2004; Bond and Bergstrom, 2006; Bergstrom et al., 2007; Moosmüller
13 et al., 2011; Kirchstetter and Thatcher, 2012; Lack et al., 2012; Bond et al., 2013; Saleh et al., 2013; Laskin
14 et al., 2015; Valenzuela et al., 2015; Devi et al., 2016). The method has been used not only for in situ
15 absorption measurements but also for interpreting absorption coefficients retrieved from remote
16 sensing measurements, such as the AERONET (e.g., Russell et al., 2010; Arola et al., 2011; Cazorla et al.,
17 2013; Feng et al., 2013; Wang et al., 2016).

18

19 One of the instruments used for measuring black carbon concentrations is the Aethalometer that
20 collects aerosol on a filter tape, measures changes in light attenuation in the wavelength range of 370
21 – 950 nm and calculates the equivalent black carbon (eBC) concentrations. The data are used also to
22 calculate α_{abs} and to estimate the contributions of fossil fuel emissions and biomass burning to eBC.
23 The Aethalometer model (Sandradewi et al., 2008a) is probably the most widely-used method for this
24 and it is even calculated automatically in the new Aethalometer model AE33. It is there assumed that
25 the absorption Ångström exponents are $\alpha_{ff} = 1$ and $\alpha_{bb} = 2$ for eBC from fossil fuel and biomass burning,
26 respectively. These are the default settings in the AE33, but also different α_{ff} and α_{bb} values have been
27 used (Sandradewi et al., 2008b; Herich et al., 2011; Fuller et al., 2014; Harrison et al., 2013; Healy et al.,
28 2017; Zotter et al., 2017; Helin et al., 2018).

29



1 The interpretation of α_{abs} is ambiguous since it not only depends on the dominant absorber but also on
2 the size and internal structure of the particles, core size and shell thickness. For instance, for pure BC
3 particles, α_{abs} may be < 1 and BC particles coated with non-absorbing material may have α_{abs} in the
4 range from < 1 to ~ 1.7 (e.g., Gyawali et al., 2009; Lack and Cappa, 2010; Lack and Langridge, 2013; Liu
5 et al., 2018; Chylek et al., 2019; Zhang et al., 2020). The present paper may be considered as an
6 extension to the above-mentioned analyses since they did not explicitly analyze the effects on the
7 Aethalometer model. The aim of this study is to estimate uncertainties of the Aethalometer-model-
8 derived fractions of absorption by eBC from fossil fuel and biomass burning when spherical BC cores
9 are coated by some non-absorbing material. Biomass-burning fractions were calculated for pure and
10 coated single particles, for lognormal unimodal and bimodal size distributions. The work is based on
11 modeling only, no measurement data are used.

12

13 2. Methods

14 The BC cores were assumed to be coated with an ammonium sulfate shell by using two approaches. It
15 was assumed 1) that the shell thickness the same for all particles in a size distribution (Fig. 1a) and 2)
16 that the core volume fraction is the same for all particles in a size distribution (Fig. 1b). The core volume
17 fraction was calculated from

$$18 \quad f_c = \frac{V_{\text{core}}}{V_p} = \left(\frac{D_{\text{core}}}{D_p} \right)^3 = \left(\frac{D_{\text{core}}}{D_{\text{core}} + 2s} \right)^3 \quad (1)$$

19 where D_p is the particle diameter ($= D_c + 2s$), D_{core} is the core diameter and s the shell thickness. The
20 shell volume fraction was then calculated from $f_s = 1 - f_c$.

21

22 Lognormal size distributions $n(D_p, D_g, \sigma_g)$ were generated where D_p is the particle diameter, D_g is the
23 geometric mean diameter and σ_g the geometric standard deviation. The D_p range was $3 \text{ nm} - 10 \mu\text{m}$.
24 For the unimodal size distributions D_g range was $50 \text{ nm} - 1 \mu\text{m}$ and σ_g was given three values 1.4, 1.6,
25 1.8 (Fig. 1c and 1d). Also bimodal size distributions were generated. For the small-particle mode the
26 geometric mean diameter D_{g1} range was $50 - 100 \text{ nm}$, and the large-particle mode D_{g2} range was 100
27 $- 500 \text{ nm}$. In addition to varying the geometric mean diameters also the ratios of the number of particles



1 in the two modes were varied. Two cases were used for this: 1) $N_1 = 10N_2$, $\sigma_{g1} = 1.4$, $\sigma_{g2} = 1.6$ (Fig. 1e)
 2 and 2) $N_1 = N_2$, $\sigma_{g1} = 1.6$, $\sigma_{g2} = 1.6$ (Fig. 1f).

3

4 Absorption coefficients were calculated from

$$5 \quad \sigma_{ap}(\lambda) = \int Q_a(\lambda, D_p, m_{core}, m_{shell}, s) \frac{\pi}{4} D_p^2 n(D_p) dD_p \quad (2)$$

6 where Q_a is the absorption efficiency that is a function of the wavelength λ , D_p , the complex refractive
 7 indices of the core and shell, m_{core} and m_{shell} , respectively, and the shell thickness s . Q_a was calculated
 8 using the N-Mie fortran code that is based on a recursive algorithm of Wu and Wang (1991). The code
 9 calculates the extinction, scattering and absorption efficiency factors for n-layered spheres. The
 10 complex refractive indices were $m_{core} = 1.85 + 0.71i$ (BC as in Lack and Cappa, 2010) and $m_{shell} = 1.52 + 0i$
 11 (ammonium sulfate) for the core and shell, respectively. Absorption coefficients were calculated for
 12 the Aethalometer wavelengths $\lambda = 470$ nm and 950 nm and α_{abs} was calculated from

$$13 \quad \alpha_{abs} = - \frac{\ln(\sigma_{ap}(\lambda = 470nm) / \sigma_{ap}(\lambda = 950nm))}{\ln(470/950)} \quad (3)$$

14 The wavelengths 470 nm and 950 nm were used as they are used also in the AE33 automatic source
 15 apportionment.

16

17 For the absorption due to particles from wood burning or biomass burning Zotter et al. (2017) give
 18 the equation

$$19 \quad \sigma_{a.bb}(\lambda_2) = \frac{\sigma_a(\lambda_1) - \sigma_a(\lambda_2) \left(\frac{\lambda_1}{\lambda_2}\right)^{-\alpha_{ff}}}{\left(\frac{\lambda_1}{\lambda_2}\right)^{-\alpha_{bb}} - \left(\frac{\lambda_1}{\lambda_2}\right)^{-\alpha_{ff}}} \quad (4)$$

20 Noting that $\sigma_a(\lambda_1) = \sigma_a(\lambda_2) (\lambda_1 / \lambda_2)^{-\alpha_{abs}}$ the fraction of absorption due to biomass burning is

$$21 \quad BB(\%) = 100\% \frac{\sigma_{a.bb}(\lambda_2)}{\sigma_a(\lambda_2)} = 100\% \frac{\left(\frac{\lambda_1}{\lambda_2}\right)^{-\alpha_{abs}} - \left(\frac{\lambda_1}{\lambda_2}\right)^{-\alpha_{ff}}}{\left(\frac{\lambda_1}{\lambda_2}\right)^{-\alpha_{bb}} - \left(\frac{\lambda_1}{\lambda_2}\right)^{-\alpha_{ff}}} \quad (5)$$



1 so that BB% depends on the Ångström exponents α_{abs} , α_{ff} and α_{bb} . Two settings for the constants were
2 used, the one presented in the AE33 manual: $\alpha_{\text{ff}} = 1$ and $\alpha_{\text{bb}} = 2$, and the one presented by Zotter et al.
3 (2017) : $\alpha_{\text{ff}} = 0.9$ and $\alpha_{\text{bb}} = 1.68$.

4

5 **3. Results and discussion**

6 **3.1 Single particles**

7 The absorption Ångström exponent α_{abs} and the fraction of biomass-burning BC for single coated
8 particles are shown in Fig. 2. The dashed lines in Figs. 2a, 2c, and 2e show the core diameter D_{core} of
9 particles that have the same diameter D_p at all shell thicknesses. In Figs. 2b, 2d and 2f the dashed lines
10 show the particle diameter D_p and f_s of particles that have the same D_{core} at all shell volume fractions
11 f_s in the range $f_s \leq 99\%$. The dependence of α_{abs} on core and shell is presented twice. This is apparently
12 superfluous but they are visualizations that complement each other.

13

14 The first approach (Figs. 2a, 2c, and 2e) shows that when $D_{\text{core}} < \sim 150$ nm and $s > \sim 25 - 50$ nm the
15 absorption Ångström exponent $\alpha_{\text{abs}} > 1.4$. The respective BB fractions are larger than about 40% or 60%
16 for the Aethalometer model parameters of $\alpha_{\text{ff}} = 1$, $\alpha_{\text{bb}} = 2$ (pair 1) and $\alpha_{\text{ff}} = 0.9$, $\alpha_{\text{bb}} = 1.68$ (pair 2),
17 respectively. Fig. 2a also shows that for $D_{\text{core}} < \sim 100$ nm there are two maxima of the α_{abs} when the
18 shell grows thicker. In the second maximum $\alpha_{\text{abs}} > \sim 1.6$. As a result the BB fractions would be $> 60\%$
19 and even $> 100\%$ for the two Aethalometer model parameter pairs. When D_{core} is in the range of ~ 170 -
20 200 nm $\alpha_{\text{abs}} \approx 1$ and α_{abs} decreases with a growing s . For larger core diameters the absorption Ångström
21 exponent is even smaller. When $D_{\text{core}} > 200$ nm $\alpha_{\text{abs}} < 1$, and even negative for $D_{\text{core}} > \sim 360$ nm. Further,
22 when $D_{\text{core}} > 200$ nm, α_{abs} does not grow essentially at all as a function of s .

23

24 The visualization of α_{abs} as a function of shell volume fraction f_s and particle full diameter D_p (Fig. 2b)
25 shows some other features. When $D_p < 50$ nm, α_{abs} varies in the range of 1.0 - 1.1 and it does not depend
26 on f_s but in the D_p range of about 100 – 300 nm α_{abs} depends strongly on f_s . When $D_p \approx 500$ nm $\alpha_{\text{abs}} <$
27 1 for almost all shell volume fractions, up to $f_s \sim 99\%$. For larger particles α_{abs} is close to 0 at all shell
28 volume fractions.

29



1 The visualization also shows that the α_{abs} value of 1, usually considered as indication of BC, is not a
2 result of an unambiguous $D_{\text{core}}-s$ (Fig. 2a) or D_p-f_s (Fig. 2b) combination.

3

4 **3.2 Unimodal BC core size distributions, same coating thickness for all sizes**

5 For single particles α_{abs} depends clearly both the core size and the shell thickness. However, in real
6 atmospheric studies the wavelength dependency of absorption by particle size distributions are
7 measured. Here these were first modeled by assuming that pure BC particle size distributions get
8 coated with ammonium sulphate layers so that the shell thickness is independent of particle size as
9 visualized in Fig. 1a. For example, the shell thickness on a 50 nm BC particle would be the same as on a
10 200 nm particle which means the shell volume fractions are not the same. The BC core geometric mean
11 diameter ($D_{g,\text{core}}$) was varied from 50 to 200 nm at 10 nm intervals. The geometric standard deviations
12 of the size distributions were $\sigma_g = 1.4$, $\sigma_g = 1.6$, and $\sigma_g = 1.8$ representing narrow, average and wide
13 size distributions. The shell thickness s varied from 0 to 250 nm at 1 nm intervals. Absorption coefficient
14 and subsequently α_{abs} was calculated for the full size distribution 3 – 2500 nm.

15

16 The results are first shown as a function of $D_{g,\text{core}}$ and shell thickness s for the three size distribution
17 widths (Fig. 3). There are both similarities and differences compared with the corresponding
18 relationships of single particles (Fig. 2). For example, for single particles $\alpha_{\text{abs}} \approx 1$ at $D_{\text{core}} \approx 180$ nm for
19 shell thicknesses $s \approx 0 - 70$ nm as shown by the almost vertical $\alpha_{\text{abs}} = 1$ isoline in Fig. 2a whereas for the
20 size distributions with $\sigma_{g,\text{core}} > 1$ the respective isoline is a strong function of both s and $\sigma_{g,\text{core}}$ (Fig. 3a).
21 At all widths of the size distribution α_{abs} increases with increasing shell thickness and then starts
22 decreasing. For small core sizes ($D_{g,\text{core}} < \sim 80$ nm) α_{abs} has also a second maximum when the size
23 distribution is narrow. The width of the size distribution has a clear effect on the α_{abs} : for all core sizes
24 and shell thicknesses α_{abs} decreases with increasing $\sigma_{g,\text{core}}$.

25

26 Both for single particles and size distributions the first maximum of α_{abs} is the smaller the larger the
27 $D_{g,\text{core}}$ and $\sigma_{g,\text{core}}$ are (Fig. 4a). The first maximum is reached at shell thickness $s \approx 70 \pm 5$ nm for all size
28 distribution widths although for single particles the variability of the shell thickness corresponding to
29 the first maximum is larger (Fig. 4b). The first maximum α_{abs} results in apparent BB fractions of up to



1 ~100% for single particles and in the range from 0 to ~80% for the size distributions and again the BB(%)
2 is the smaller the larger the $D_{g,core}$ and σ_g are (Fig. 4c and d).

3
4 This approach is further followed by plotting the parameters as a function of shell thickness for three
5 different BC core diameters, 50 nm, 70 nm, and 90 nm of single particles and core size distributions
6 with the geometric standard deviations of $\sigma_{g,core} = 1.4, 1.6, \text{ and } 1.8$ (Fig. 5). This analysis can be
7 considered as a description of what may happen to the size distribution, α_{abs} and the apparent BB(%)
8 during condensational growth on fresh small BC cores if the growing shell thickness were independent
9 of the core diameter, even if this is unrealistic. The shell volume fraction f_s increases to $> 99.9\%$ when
10 the shell thickness grows from $s = 0$ nm to 250 nm on single 50 nm particles but to lower fractions for
11 the wider size distributions and larger core sizes so that for $D_{g,core} = 90$ m and $\sigma_g = 1.8$ $f_s \approx 98\%$ even
12 with $s = 250$ nm (Fig. 5a). The geometric mean diameter D_g of the whole size distribution grows to ~600
13 nm when the shell thickness grows to 250 nm, minimal differences between the original widths (Fig.
14 5b). The width of the size distribution, i.e., σ_g decreases fast to < 1.2 (Fig. 4c). Such values correspond
15 to very narrow size distributions, not really observed in the real atmosphere.

16

17 The number-weighted D_p -to- D_{core} ratio

18
$$R_{N(D_p)} = \frac{\sum N_i R_i}{N_{tot}} = \frac{\sum N_i (D_{p,i} / D_{c,i})}{N_{tot}} \quad (6)$$

19 was calculated for the size range 90-600 nm to present the numbers comparable with papers that
20 present shell-to-core ratios of refractory BC (rBC) obtained from SP2 measurements. For instance,
21 Kondo et al. (2011) measured urban air of Tokyo and obtained the median $R = 1.1$ with a range up to
22 about 1.3, the mean $D_g = 64 \pm 6$ nm, and $\sigma_g = 1.66 \pm 0.12$. Moteki et al. (2007) conducted SP2
23 measurements in an aircraft in urban plumes on the Japanese coast. They fitted the data with lognormal
24 size distributions with mass median diameters (MMD) of 190 and 210 nm and σ_g of 1.55 and 1.45 for
25 fresh and aged rBC, respectively. The fresh rBC was thinly coated with $R < 2$ and the aged rBC thickly
26 coated with $R \sim 2$. The MMD and σ_g values yield $D_g = 107$ nm and 139 nm. Shiraiwa et al. (2008)
27 measured the mixing state and size distribution of BC aerosol with an SP2 at a remote island (Fukue) in
28 Japan. They observed that the BC number median diameters were in the range of 120–140 nm in every



1 air mass type and the median shell/core diameter ratio (R) in different air masses varied in the range of
2 1.2 – 1.6. However, they also observed that the fraction of R values in the range 2 – 3.5 was not
3 negligible either (Fig. 9 of Shiraiwa et al., 2008). Such values correspond to the range where α_{abs} first
4 grows to >1.6 for the narrow ($\sigma_{g,\text{core}} = 1.4$) BC core size distribution that has the smallest geometric
5 mean size ($D_{g,\text{core}} = 50$ nm) but to lower values for the wider size distributions that have larger $D_{g,\text{core}}$
6 (Fig. 5c and 5d). The first maximum is reached at shell thicknesses of $s \approx 70$ nm that corresponds to $R \approx$
7 2 and shell volume fractions of $f_s \approx 90 \pm 8\%$ (Fig. 5b). Schwarz et al. (2008) reported statistics of rBC
8 mass size distributions in urban aerosol: $f_s = 9 \pm 6\%$, $s = 20 \pm 10$ nm, MMD = 170 nm, and σ_g of 1.71
9 which yields $D_g = 72$ nm; in biomass burning emissions: $f_s = 70 \pm 9\%$, $s = 65 \pm 12$ nm, MMD = 210 nm,
10 $\sigma_g = 1.43$ which yields $D_g = 143$ nm and in background continental aerosol: $f_s = 46 \pm 3\%$, $s = 48 \pm 14$ nm,
11 MMD = 210 nm, 1.55 which yields $D_g = 118$ nm.

12

13 The referenced studies show that the s , R , and f_s values are in the range observed in ambient
14 measurements studies. What is not realistic in atmospheric aerosol is the width of the size distribution,
15 which soon decreases to $\sigma_g < 1.2$ (Fig. 5c).

16

17 After reaching the first maximum α_{abs} decreases and for single particles and the narrowest core size
18 distributions starts again growing and reaches a second maximum at shell thicknesses of $s \approx 170$ nm
19 that corresponds to $R > 4$ and $f_s > 98\%$. Such s and R values are not in the range observed in the above-
20 mentioned studies, nor are the low geometric standard deviations of $\sigma_g < 1.1$ realistic so the second
21 maximum can be considered as a theoretical value only. For size distributions with $D_{g,\text{core}} > 70$ nm there
22 is no second maximum α_{abs} .

23

24 As α_{abs} increases and decreases it is clear that this applies to BB(%) as well (Fig. 5d-e). For the smallest
25 core sizes ($D_{g,\text{core}} = 50$ nm) and the narrowest size distributions ($\sigma_{g,\text{core}} = 1.4$) the first maximum BB(%)
26 may be as high as $\sim 90\%$ when the values of $\alpha_{\text{ff}} = 0.9$, $\alpha_{\text{bb}} = 1.68$ are used in Eq. (5) but lower, $\sim 50\%$
27 when the values of $\alpha_{\text{ff}} = 1$, $\alpha_{\text{bb}} = 2$ are used. For the wider core size distributions the BB(%) fractions are
28 lower. For the widest core size distributions ($\sigma_{g,\text{core}} = 1.8$) clearly positive BB(%) values are reached only
29 for the smallest core sizes.



1

2 Fig. 5 can also be considered as a proxy for a time series of the development of α_{abs} and derived BB(%)
3 after emission of BC particles and their growth by condensation of nonabsorbing compounds. Similar
4 development – α_{abs} increase to > 1.3 and decrease to < 0.9 during a several-day-long pollution episode
5 during which the D_g of the whole size distribution grew possibly by condensation – was observed at
6 SORPES in Nanjing, China (Fig. 9 of Shen et al., 2018). There was no SP2 available for the core-shell
7 structure measurements in that study so it cannot really be proven that the observed α_{abs} development
8 was due to condensational growth even though it seems a good explanation and is qualitatively in line
9 with Fig. 5.

10

11 **3.3 Unimodal size distributions with the same BC core fraction for all sizes**

12 The second approach is to assume that the BC core fraction – or equivalently the shell volume fraction
13 – is the same for all sizes which means that the shell thickness increases with size as was visualized in
14 Fig. 1b. This can be considered to be a result of aging of BC by not only condensational growth but also
15 by cloud processing. The latter would lead to thick shells on particles activated into cloud droplets that
16 would absorb for instance SO_2 and NH_3 and that would not rain but get later back into the aerosol phase
17 by evaporation of cloud water. The constant volume fraction is not realistic but neither is the constant
18 shell thickness. Both can be considered to be approximations.

19

20 In this approach the geometric standard deviations of the whole size distributions were set to $\sigma_g = 1.4$,
21 1.6 and 1.8 and the shell volume fractions to vary from 0% to 99%. The resulting α_{abs} and BB(%) are
22 presented as a function of D_g , f_s and σ_g (Fig. 6). They are comparable with the analogous plots for single
23 particles, i.e., $\sigma_g = 1.0$ (Fig. 2b, 2d, and 2f). Several observations can be made from Fig. 6. One of them
24 is that the isoline of $\alpha_{\text{abs}} = 1$ grows with growing D_g for each of the size distribution widths (σ_g) but
25 decreases with growing σ_g . Another is that the wider the size distribution is, the lower are the α_{abs} and
26 BB(%) at any given shell volume fraction. The third one is that for all three widths α_{abs} and BB(%) grows
27 when f_s grows but that the growth is not uniformly distributed over the f_s vs. D_g space.

28



1 The last observation leads to calculations of size-dependent sensitivities of α_{abs} to variations in f_s . The
2 sensitivity was calculated as $d\alpha_{\text{abs}}/df_s$ and its unit is $\%^{-1}$. Fig. 7a shows the sensitivities in the whole f_s
3 range of 1 - 99% as a function of D_g for the three size distribution widths. The sensitivity depends clearly
4 on both D_g and σ_g of the size distribution and it also varies with f_s . It is very clear that α_{abs} is most
5 sensitive to f_s variations when D_g of the size distribution is in the accumulation mode sizes of 100 – 200
6 nm. The sensitivity grows fairly steadily with growing f_s until for $f_s > 90\%$ it increases very strongly.

7

8 Another step for visualizing the sensitivities was taken by calculating size-dependent average
9 sensitivities of α_{abs} and BB(%) in three f_s ranges: $f_s = 0 - 50\%$, $50 - 90\%$ and $90 - 99\%$ (Fig. 7b and 7c).
10 These lines can be used for a rough estimate on a possible effect on α_{abs} and BB(%). For instance, if D_g
11 ≈ 140 nm, $\sigma_g = 1.4$, and $f_s \approx 50 - 90\%$, an increase of f_s from 50% to 51% leads to an α_{abs} increase of
12 ~ 0.01 and consequently to a BB(%) increase of $\sim 1\%$ when Aethalometer model constants of $\alpha_{\text{ff}} = 0.9$,
13 $\alpha_{\text{bb}} = 1.68$ are used.

14

15 **3.4 Bimodal size distributions with the same BC core fraction for all sizes in the mode**

16 Finally, bimodal size distributions are examined briefly. The size distributions consist of two externally
17 mixed modes that have different shell volume fractions. In both modes the shell volume fractions are
18 size-independent as in Fig. 1b. Mode 1 is an Aitken mode with the geometric mean diameter D_{g1} in the
19 range 50 – 100 nm. There are two different settings for the Aitken mode: in the first case its number
20 concentration is 10 times larger than that of the accumulation mode, i.e., $N_1 = 10N_2$, it consists of almost
21 pure fresh BC particles with $f_{s1} = 5\%$ and it is narrow, $\sigma_{g1} = 1.4$. In the second setting the number
22 concentrations of the Aitken and accumulation mode are equal ($N_1 = N_2$), the Aitken mode is aged so
23 that $f_{s1} = 50\%$ and it is wider, $\sigma_{g1} = 1.6$. Mode 2 is an accumulation mode with the geometric mean
24 diameter D_{g2} in the range 100 – 500 nm, $\sigma_{g2} = 1.6$ and it is very aged, with $f_{s2} = 98\%$. The accumulation
25 mode could be result of cloud processing as explained above.

26

27 The results show that α_{abs} is more sensitive to variations of the accumulation mode than of the Aitken
28 mode (Fig. 8a). For instance, if $D_{g2} < 250$ nm, $\alpha_{\text{abs}} > 1$ at all $D_{g,1}$ values. Also, if $D_{g,1} = 60$ nm and D_{g2} varies
29 in the whole range of 100 – 500 nm, α_{abs} varies in the range of $\sim 0.4 - 1.3$. When the Aitken mode



1 dominates the number concentration ($N_1 = 10N_2$) with the fresh BC particles the maximum $\alpha_{\text{abs}} \approx 1.2$ at
2 $D_{g1} \approx 60$ nm and $D_{g2} \approx 140$ nm is smaller than when the two modes have equal amount of particles. In
3 the latter case the maximum $\alpha_{\text{abs}} > 1.3$. When the Aitken mode with $f_s = 5\%$ dominates the number
4 concentration the whole size distribution moves to the region that is less sensitive to f_s variations as
5 discussed above in section 3.3. It is worth noting also that the maximum α_{abs} and BB(%) values (Fig. 8b
6 and 8c) are smaller than derived from the unimodal size distributions (section 3.3).

7

8 **4. Summary and conclusions**

9 The purpose of this study is not to claim that all Aethalometer model results are wrong. It is clear that
10 there are BrC particles that have absorption Ångström exponents clearly larger than one, as shown in a
11 very large number of publications. However, the size of light-absorbing particles and their coating even
12 by purely scattering material affect clearly the wavelength dependence of absorption and thus have
13 the potential to affect the Aethalometer model results. Since the wavelength dependency is used for
14 source apportionment these effects have the potential to result in tens of percent too high or low
15 contributions of wood-burning or fossil fuel emissions.

16

17 There are some important results. α_{abs} equals 1 in very rare cases and thus BB(%) was very seldom 0%
18 even though BC was the only absorbing material in the simulations. The shape of size distribution plays
19 an important role. Narrow size distributions result in higher α_{abs} and BB(%) values than wide size
20 distributions. The sensitivity of α_{abs} and BB(%) to variations in shell volume fractions is the highest for
21 accumulation mode particles. This is important because that is where the largest aerosol mass is. For
22 the interpretation of absorption Ångström exponents it would be very good to measure BC size
23 distributions and shell thicknesses together with the wavelength dependency of absorption.

24

25 There are obvious limitations in this study. A core-shell Mie model was used only so the work is limited
26 to spherical particles. And further, even if particles were spherical how well can they be modeled with
27 a Mie code when they are collected on filters? Or does light absorption then follow the spectral
28 absorbance of the bulk materials? This question could in principle be answered by generating spherical
29 BC particles, coating them in an aging chamber with some non-absorbing material, for instance



1 ammonium sulfate, and measuring both light absorption at multiple wavelengths with an Aethalometer
2 and BC core size distributions and shell thicknesses with an SP2. If α_{abs} increased up to some maximum
3 value as a function of shell thickness and then started decreasing like in the simulations above, then
4 the uncertainties discussed in this work should be taken seriously. On the other hand, if none of these
5 effects were observed and the absorption Ångström exponents of the collected particles were ≈ 1
6 regardless of core size and shell thickness it would be safe to say that the Aethalometer measures the
7 absorption spectra of the bulk materials and that the Aethalometer model yields correct results.
8 Probably the truth is somewhere between these extremes: when the filter tape is still relatively clean
9 the particles can be modeled even with a Mie code and for heavily-load filters α_{abs} is that of bulk
10 material. Also this could be tested experimentally.

11

12 *Acknowledgements* This work was supported by the Academy of Finland via project NABCEA (grant
13 no. 296302) and by Business Finland via project BC Footprint (grant no. 49402-201040).

14

15 **References**

16 Andreae, A. and Gelencser, A.: Black carbon or brown carbon? The nature of light-absorbing
17 carbonaceous aerosols, *Atmos. Chem. Phys.*, 6, 3131–3148, [http://www.atmos-chem-](http://www.atmos-chem-phys.net/6/3131/2006)
18 [phys.net/6/3131/2006](http://www.atmos-chem-phys.net/6/3131/2006), 2006.

19

20 Arola, A., Schuster, G., Myhre, G., Kazadzis, S., Dey, S., and Tripathi, S. N.: Inferring absorbing organic
21 carbon content from AERONET data, *Atmos. Chem. Phys.*, 11, 215–225, [https://doi.org/10.5194/acp-](https://doi.org/10.5194/acp-11-215-2011)
22 [11-215-2011](https://doi.org/10.5194/acp-11-215-2011), 2011.

23

24 Bergstrom, R.W., Pilewskie, P., Russell, P. B., Redemann, J., Bond, T., Quinn, P. K., and Sierau, B.: Spectral
25 Absorption Properties of Atmospheric Aerosols, *Atmos. Chem. Phys.*, 7, 5937–5943,
26 <http://www.atmos-chem-phys.net/7/5937/2007>, 2007.

27

28 Bond, T. C. and Bergstrom, R. W.: Light Absorption by Carbonaceous Particles: An Investigative
29 Review, *Aerosol Sci. Technol.*, 40, 27–67, 2006.



1
2 Bond, T. C., Doherty, S. J., Fahey, D. W., Forster, P. M., Berntsen, T., DeAngelo, B. J., Flanner, M. G.,
3 Ghan, S., Kärcher, B., Koch, D., Kinne, S., Kondo, Y., Quinn, P. K., Sarofim, M. C., Schultz, M.
4 G., Schulz, M., Venkataraman, C., Zhang, H., Zhang, S., Bellouin, N., Guttikunda, S. K., Hopke, P. K.,
5 Jacobson, M. Z., Kaiser, J. W., Klimont, Z., Lohmann, U., Schwarz, J. P., Shindell, D., Storelvmo, T.,
6 Warren, S. G., and Zender, C.S.: Bounding the role of black carbon in the climate system: A scientific
7 assessment, *J. Geophys. Res. Atmos.*, 118, 2013.
8
9 Cazorla, A., Bahadur, R., Suski, K. J., Cahill, J. F., Chand, D., Schmid, B., Ramanathan, V., and Prather, K.
10 A.: Relating aerosol absorption due to soot, organic carbon, and dust to emission sources determined
11 from in-situ chemical measurements, *Atmos. Chem. Phys.*, 13, 9337–9350,
12 <https://doi.org/10.5194/acp-13-9337-2013>, 2013.
13
14 Chylek, P., Lee, J. E., Romonosky, D. E., Gallo, F., Lou, S., Shrivastava, M., et al.: Mie scattering captures
15 observed optical properties of ambient biomass burning plumes assuming uniform black, brown, and
16 organic carbon mixtures. *J. Geophys. Res., Atmospheres*, 124, 11406–11427.
17 <https://doi.org/10.1029/2019JD031224>, 2019.
18
19 Devi, J.J., Bergin, M., McKenzie, M., Schauer, J.J., and Weber, R.: Contribution of particulate brown
20 carbon to light absorption in the rural and urban Southeast US, *Atmos. Environ.*, 136, 95 - 104, 2016.
21
22 Feng, Y., Ramanathan, V., and Kotamarthi, V. R.: Brown carbon: a significant atmospheric absorber of
23 solar radiation?, *Atmos. Chem. Phys.*, 13, 8607–8621, <https://doi.org/10.5194/acp-13-8607-2013>,
24 2013.
25
26 Fuller, G.W., Tremper, A.H., Baker, T.D., Yttri, K.E., Butterfield, D.: Contribution of wood burning to
27 PM10 in London. *Atmos. Environ.* 87, 87–94, 2014.
28



- 1 Gyawali, M., Arnott, W. P., Lewis, K., and Moosmüller, H.: In situ aerosol optics in Reno, NV, USA during
2 and after the summer 2008 California wildfires and the influence of absorbing and non-absorbing
3 organic coatings on spectral light absorption, *Atmos. Chem. Phys.*, 9, 8007-8015, doi:10.5194/acp-9-
4 8007-2009, 2009.
- 5
- 6 Harrison, R.M., Beddows, D.C., Jones, A.M., Calvo, A., Alves, C., Pio, C.: An evaluation of some issues
7 regarding the use of aethalometers to measure woodsmoke concentrations. *Atmos. Environ.* 80, 540–
8 548, 2013.
- 9
- 10 Healy, R., Sofowote, U., Su, Y., Deboasz, J., Noble, M., Jeong, C.-H., Wang, J., Hilker, N., Evans, G.,
11 Doerksen, G.: Ambient measurements and source apportionment of fossil fuel and biomass burning
12 black carbon in Ontario. *Atmos. Environ.* 161, 34–47, 2017.
- 13
- 14 Helin, A., Niemi, J., Virkkula, A., Pirjola, L., Teinilä, K., Backman, J., Aurela, M., Saarikoski, S., Rönkkö, T.,
15 Asmi, E., Timonen, H.: Characteristics and source apportionment of black carbon in the Helsinki
16 metropolitan area, Finland, *Atmos. Environ.*, 190, 87 – 98, doi: 10.1016/j.atmosenv.2018.07.022, 2018.
- 17
- 18 Herich, H., Hueglin, C., and Buchmann, B.: A 2.5 year’s source apportionment study of black carbon
19 from wood burning and fossil fuel combustion at urban and rural sites in Switzerland, *Atmos. Meas.*
20 *Tech.*, 4, 1409–1420, doi:10.5194/amt-4-1409-2011, 2011.
- 21
- 22 Kirchstetter, T. W., Novakov, T., and Hobbs, P. V.: Evidence that the spectral dependence of
23 light absorption by aerosols is affected by organic carbon, *J. Geophys. Res.*, 109, D21208,
24 doi:10.1029/2004JD004999, 2004.
- 25
- 26 Kirchstetter, T. W. and Thatcher, T. L.: Contribution of organic carbon to wood smoke particulate matter
27 absorption of solar radiation, *Atmos. Chem. Phys.*, 12, 6067–6072, doi:10.5194/acp-12-6067-2012,
28 2012.
- 29



- 1 Kondo, Y., L. Sahu, N. Moteki, F. Khan, N. Takegawa, X. Liu, M. Koike, and T. Miyakawa: Consistency and
2 traceability of black carbon measurements made by laser-induced incandescence, thermal-optical
3 transmittance, and filter-based photo-absorption techniques, *Aerosol Sci. Technol.*, 45, 295–312,
4 doi:10.1080/02786826.2010.533215, 2011.
- 5
- 6 Lack, D. A. and Cappa, C. D.: Impact of brown and clear carbon on light absorption enhancement,
7 single scatter albedo and absorption wavelength dependence of black carbon, *Atmos. Chem. Phys.*,
8 10, 4207–4220, doi:10.5194/acp-10-4207-2010, 2010.
- 9
- 10 Lack, D. A. and Langridge, J. M.: On the attribution of black and brown carbon light absorption using
11 the Ångström exponent, *Atmos. Chem. Phys.*, 13, 10535–10543, [https://doi.org/10.5194/acp-13-](https://doi.org/10.5194/acp-13-10535-2013)
12 10535-2013, 2013.
- 13
- 14 Lack, D. A., Langridge, J. M., Bahreini, R., Cappa, C. D., Middlebrook, A. M., and Schwarz, J. P.: Brown
15 carbon and internal mixing in biomass burning particles, *P. Natl. Acad. Sci. USA*, 109, 14802–14807,
16 2012.
- 17
- 18 Laskin, A., Laskin, J., and Nizkorodov, S. A.: Chemistry of Atmospheric Brown Carbon, *Chem.*
19 *Rev.*, 115, 4335–4382, <https://doi.org/10.1021/cr5006167>, 2015.
- 20
- 21 Liu, C., Chung, C. E., Yin, Y., and Schnaiter, M.: The absorption Ångström exponent of black carbon:
22 from numerical aspects, *Atmos. Chem. Phys.*, 18, 6259–6273, [https://doi.org/10.5194/acp-18-6259-](https://doi.org/10.5194/acp-18-6259-2018)
23 2018, 2018.
- 24
- 25 Moosmüller, H., Chakrabarty, R. K., Ehlers, K. M., and Arnott, W. P.: Absorption Ångström coefficient,
26 brown carbon, and aerosols: basic concepts, bulk matter, and spherical particles, *Atmos. Chem. Phys.*,
27 11, 1217–1225, doi:10.5194/acp-11-1217-2011, 2011.
- 28



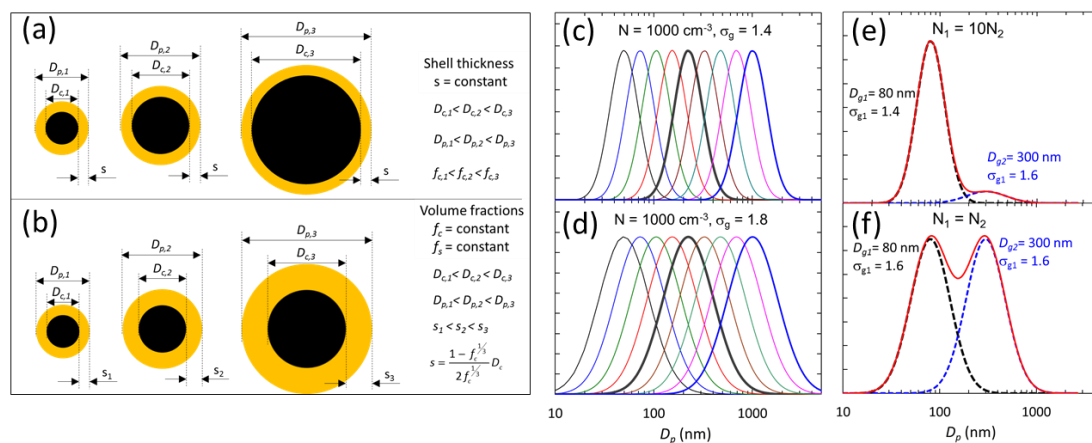
- 1 Moteki, N., Y. Kondo, Y. Miyazaki, N. Takegawa, Y. Komazaki, G. Kurata, T. Shirai, D. R. Blake, T.
2 Miyakawa, and Koike, M.: Evolution of mixing state of black carbon particles: Aircraft measurements
3 over the western Pacific in March 2004, *Geophys. Res. Lett.*, 34, L11803, doi:10.1029/2006GL028943,
4 2007.
5
- 6 Russell, P., Bergstrom, R., Shinozuka, Y., Clarke, A., Decarlo, P., Jimenez, J., Livingston, J., Redemann,
7 J., Dubovik, O., and Strawa, A.: Absorption Angstrom Exponent in AERONET and related data as an
8 indicator of aerosol composition, *Atmos. Chem. Phys.*, 10, 1155-1169, 2010.
9
- 10 Saleh, R., Hennigan, C., McMeeking, G., Chuang, W., Robinson, E., Coe, H., Donahue, N., Robinson, A.:
11 Absorptivity of brown carbon in fresh and photo-chemically aged biomass-burning emissions. *Atmos.*
12 *Chem. Phys.* 13, 7683–7693, 2013.
13
- 14 Sandradewi, J., Prevot, A. S. H., Szidat, S., Perron, N., Alfarra, M. R., Lanz, V. A., Weingartner, E., and
15 Baltensperger, U.: Using aerosol light absorption measurements for the quantitative determination of
16 wood burning and traffic emission contributions to particulate matter, *Environ. Sci. Technol.*, 42, 3316–
17 3323, 2008a.
18
- 19 Sandradewi, J., Prevot, A. S. H., Weingartner, E., Schmidhauser, R., Gysel, M., and Baltensperger, U.:
20 A study of wood burning and traffic aerosols in an Alpine valley using a multi-wavelength Aethalometer,
21 *Atmos. Environ.*, 42, 101–112, 2008b.
22
- 23 Schwarz, J. P., Gao, R. S., Spackman, J. R., Watts, L. A., Thomson, D. S., Fahey, D. W., Ryerson, T. B.,
24 Peischl, J., Holloway, J. S., Trainer, M., Frost, G. J., Baynard, T., Lack, D. A., de Gouw, J. A., Warneke,
25 C., and Del Negro, L. A.: Measurement of the mixing state, mass, and optical size of individual black
26 carbon particles in urban and biomass burning emissions, *Geophys. Res. Lett.*, 35, L13810,
27 doi:10.1029/2008GL033968, 2008.
28



- 1 Shen, Y., Virkkula, A., Ding, A., Wang, J., Chi, X., Nie, W., Qi, X., Huang, X., Liu, Q., Zheng, L., Xu, Z., Petäjä,
2 T., Aalto, P. P., Fu, C., and Kulmala, M.: Aerosol optical properties at SORPES in Nanjing, east China,
3 Atmos. Chem. Phys., 18, 5265–5292, <https://doi.org/10.5194/acp-18-5265-2018>, 2018.
- 4
- 5 Shiraiwa, M., Y. Kondo, N. Moteki, N. Takegawa, L. K. Sahu, A. Takami, S. Hatakeyama, S. Yonemura,
6 and D. R. Blake: Radiative impact of mixing state of black carbon aerosol in Asian outflow, J. Geophys.
7 Res., 113, D24210, doi:10.1029/2008JD010546, 2008.
- 8
- 9 Valenzuela, A., Olmo, F.J., Lyamani, H., Antón, M., Titos, G., Cazorla, A., Alados-Arboledas, L.: Aerosol
10 scattering and absorption Angström exponents as indicators of dust and dust-free days over Granada
11 (Spain). Atmos Res., 154, pp. 1-13. 2015.
- 12
- 13 Wang, X., Heald, C. L., Sedlacek, A. J., de Sá, S. S., Martin, S. T., Alexander, M. L., Watson, T. B., Aiken,
14 A. C., Springston, S. R., and Artaxo, P.: Deriving brown carbon from multiwavelength absorption
15 measurements: method and application to AERONET and Aethalometer observations, Atmos.
16 Chem. Phys., 16, 12733–12752, <https://doi.org/10.5194/acp-16-12733-2016>, 2016.
- 17
- 18 Wu Z.P., Wang Y.P.: Electromagnetic scattering for multilayered spheres: recursive algorithms, Radio
19 Science, 26, 1393-1401, 1991.
- 20
- 21 Zhang, X., Mao, M., Yin, Y., and Tang, S.: The absorption Ångström exponent of black carbon with brown
22 coatings: effects of aerosol microphysics and parameterization, Atmos. Chem. Phys., 20, 9701–9711,
23 <https://doi.org/10.5194/acp-20-9701-2020>, 2020.
- 24
- 25 Zotter, P., Herich, H., Gysel, M., El-Haddad, I., Zhang, Y., Močnik, G., Hüglin, C., Baltensperger, U., Szidat,
26 S., and Prévôt, A. S. H.: Evaluation of the absorption Ångström exponents for traffic and wood burning
27 in the Aethalometer-based source apportionment using radiocarbon measurements of ambient
28 aerosol, Atmos. Chem. Phys., 17, 4229-4249, <https://doi.org/10.5194/acp-17-4229-2017>, 2017.
- 29



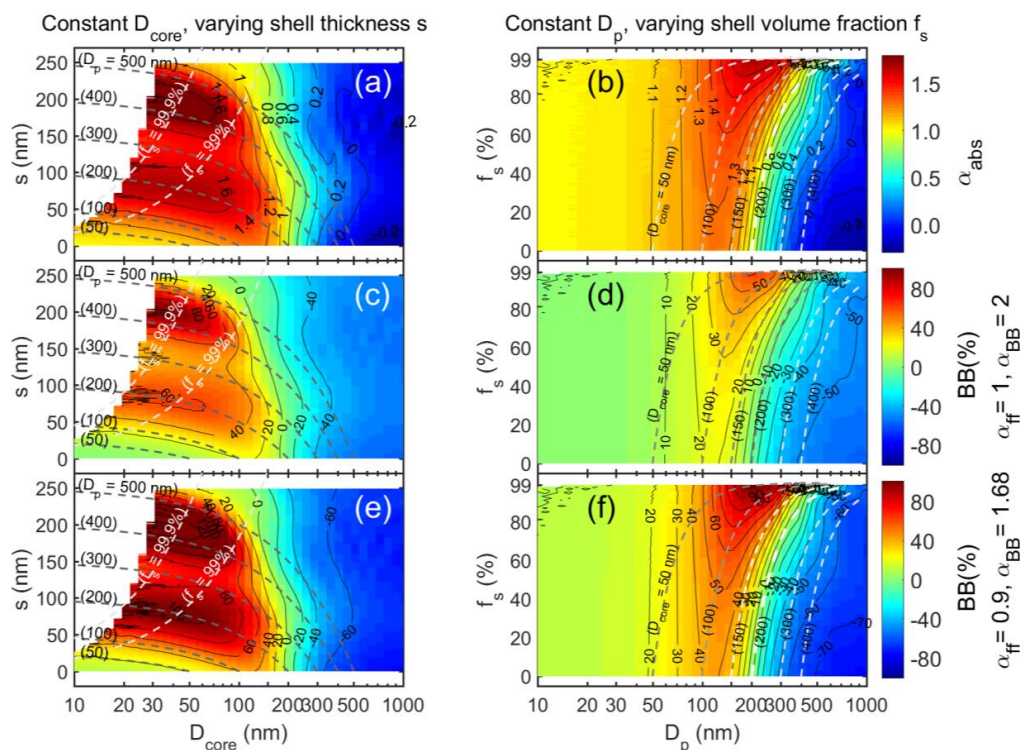
1 Figures



2

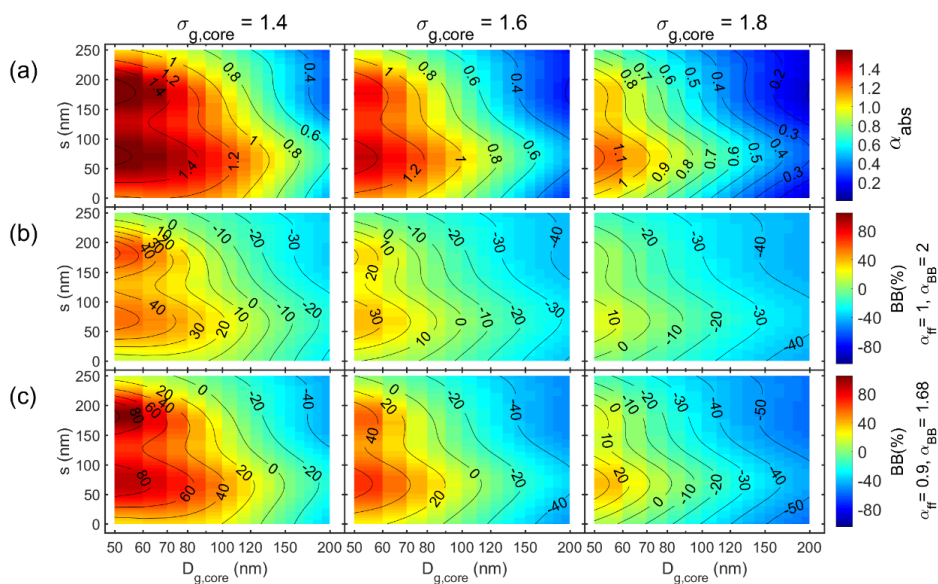
3 Figure 1. Examples of particles and size distributions used in the simulations: a) particles with a BC core
 4 coated with a constant shell thickness s , b) particles with constant BC core and shell volume fractions f_c
 5 and f_s , c) unimodal narrow size distributions with the geometric standard deviation of $\sigma_g = 1.4$, d)
 6 unimodal wide size distributions with $\sigma_g = 1.8$, e) bimodal size distributions with a dominating Aitken
 7 mode, f) bimodal size distributions with equal-sized Aitken and accumulation modes.

8

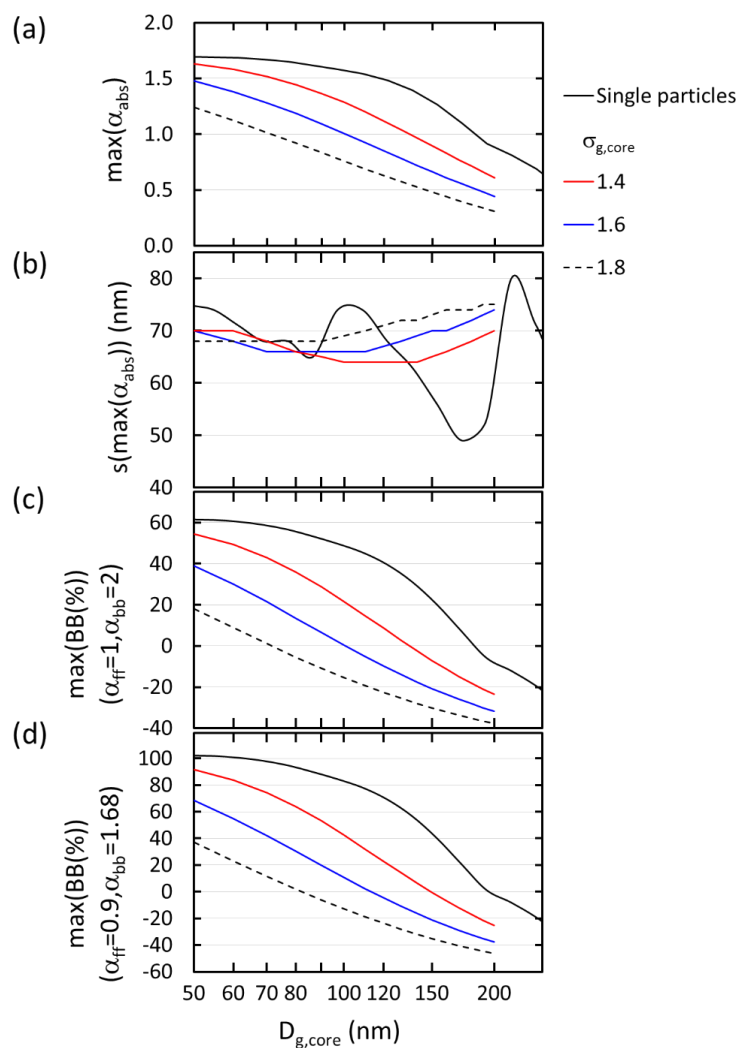


1
 2 Figure 2. Absorption Ångström exponent (α_{abs}) and the from it calculated fraction of biomass-burning
 3 BC for single coated particles as a function of (in -a, c, and e) BC core diameter (D_{core}) and shell thickness
 4 (s) and (b, d, and f) as a function of particle diameter ($D_p = D_{core} + 2s$) and shell volume fraction f_s in the
 5 range $f_s \leq 99\%$. In a), c) and e) the dark dashed lines show the D_{core} and s of particles that have the
 6 same D_p – written in parentheses – at all shell thicknesses and the light dashed line show the shell
 7 thicknesses that correspond to $f_s = 99\%$ and 99.9% . In b), d) and f) the dashed lines show the D_p and f_s
 8 of particles that have the same D_{core} – written in parentheses – at all shell volume fractions. The color
 9 bars are common for a and b, c and d, and e and f.

10
 11

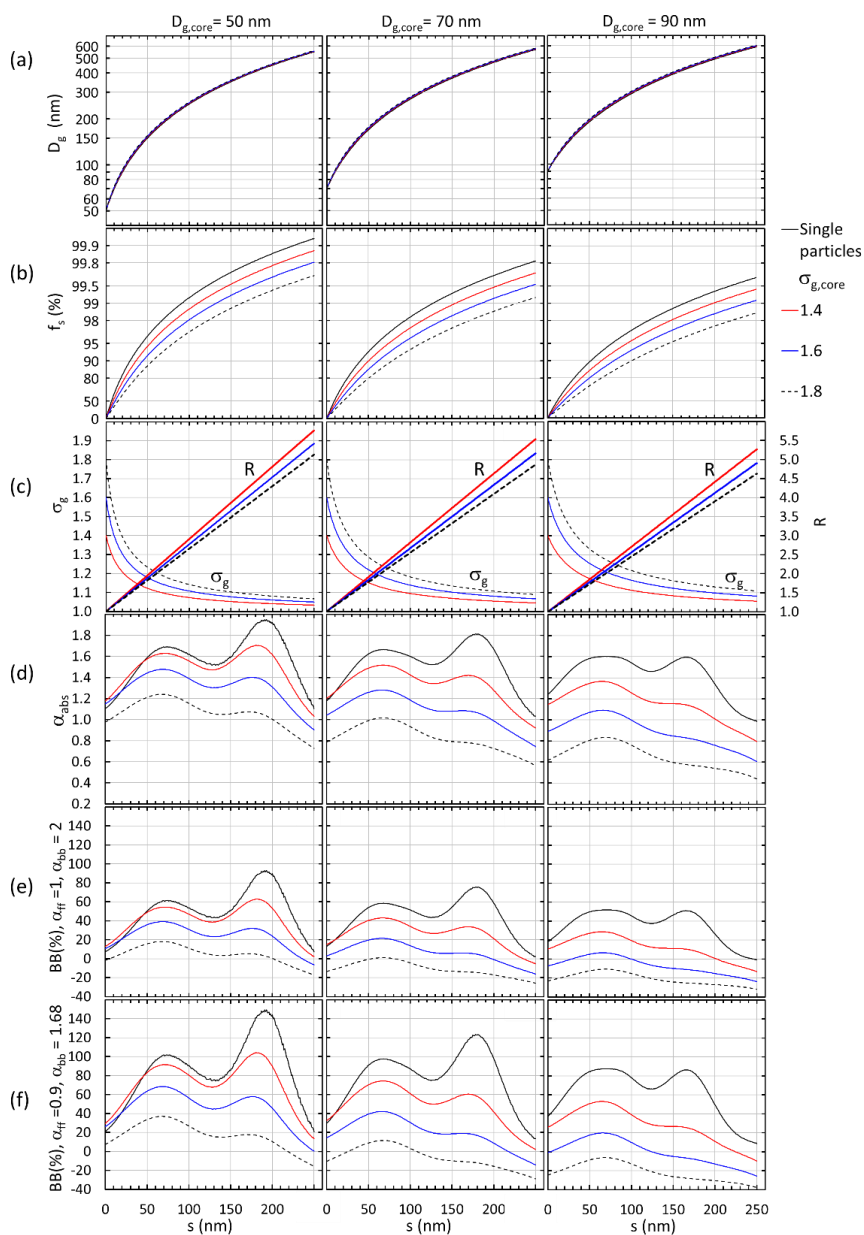


1
 2 Figure 3. Unimodal particle size distributions with a size-independent shell thickness (s) for three widths
 3 of the core size distributions: $\sigma_{g,core} = 1.4, 1.6$ and 1.8 . a) absorption Ångström exponent (α_{abs}) and the
 4 from it calculated fraction of biomass-burning BC (BB(%)) with the Aethalometer model constants of b)
 5 $\alpha_{ff} = 1, \alpha_{bb} = 2$ and c) $\alpha_{ff} = 0.9, \alpha_{bb} = 1.68$ vs. the geometric mean diameter of the core ($D_{g,core}$).

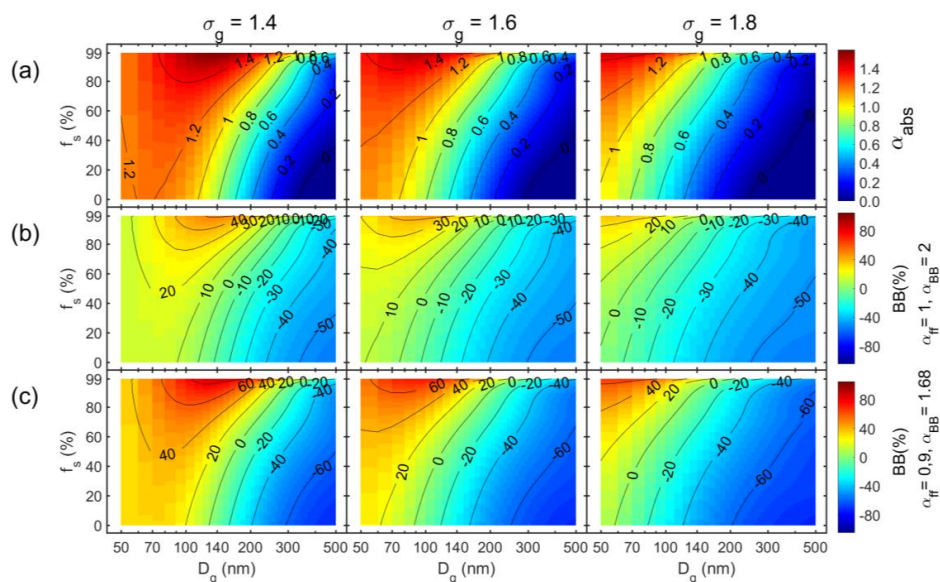


1
 2
 3
 4
 5
 6
 7
 8
 9

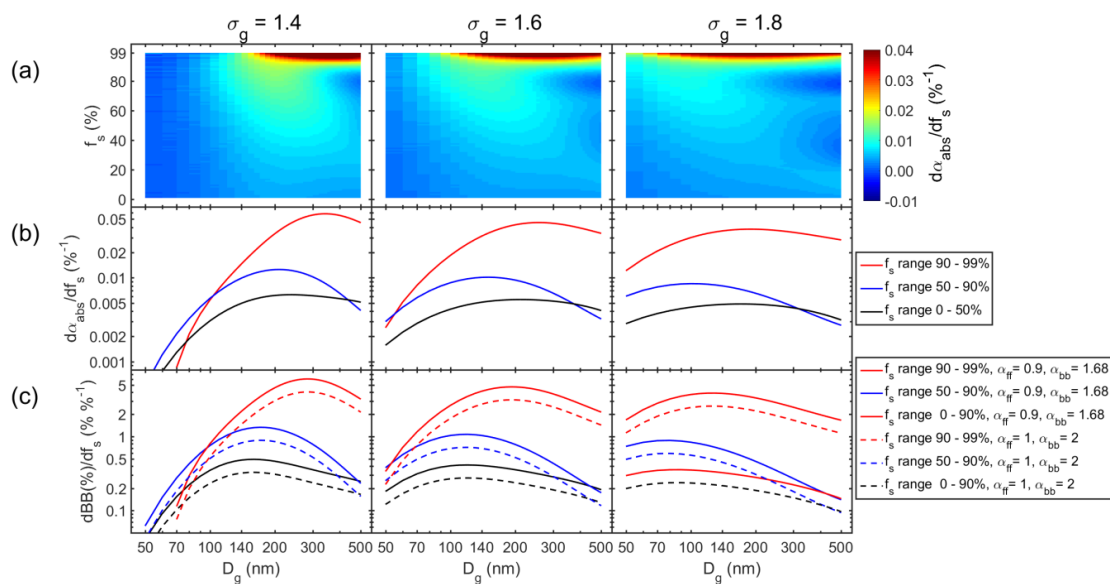
Figure 4. Size distribution dependence of the first maximum of α_{abs} when a size-independent shell grows on a BC core: a) the first maximum value of α_{abs} , b) the shell thickness at the maximum α_{abs} , c) maximum biomass-burning fraction with the Aethalometer model constants $\alpha_{ff} = 1$ and $\alpha_{bb} = 2$, and d) maximum biomass-burning fraction with the Aethalometer model constants $\alpha_{ff} = 0.9$ and $\alpha_{bb} = 1.68$ as a function of the geometric mean diameter ($D_{g,core}$) and the geometric standard deviation ($\sigma_{g,core}$) of the BC core.



1
 2 Figure 5. Examples of the growth of a non-size-dependent scattering shell on BC core size distributions
 3 with $D_{g,core} = 50$ nm, 70 nm and 90 nm. a) Geometric mean diameter, b) shell volume fraction, c)
 4 geometric standard deviation and D_p -to- D_{core} ratio (R), d) absorption Ångström exponent, e) BB(%) with
 5 the Aethalometer model constants $\alpha_{ff} = 1$ and $\alpha_{bb} = 2$, and d) biomass-burning fraction with the
 6 Aethalometer model constants $\alpha_{ff} = 0.9$ and $\alpha_{bb} = 1.68$ as a function shell thickness s .



1
 2 Figure 6. Unimodal particle size distributions with size-independent shell volume fractions f_s and three
 3 widths of the size distributions: $\sigma_g = 1.4, 1.6$ and 1.8 . a) absorption Ångström exponent (α_{abs}) and the
 4 from it calculated fraction of biomass-burning BC (BB(%)) with the Aethalometer model constants of b)
 5 $\alpha_{ff} = 1, \alpha_{bb} = 2$ and c) $\alpha_{ff} = 0.9, \alpha_{bb} = 1.68$ vs. the geometric mean diameter of the whole size distribution
 6 (D_g).
 7



1

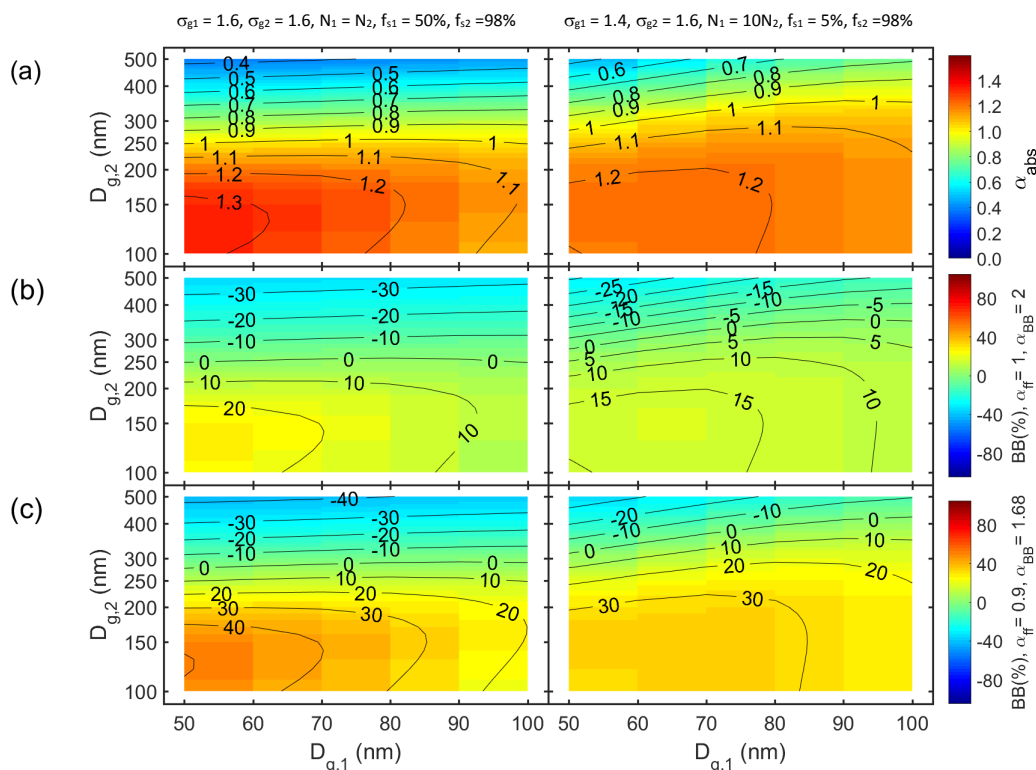
2 Figure 7. Size-dependent sensitivity of α_{abs} and BB(%) to variations of the shell volume fraction f_s . a) α_{abs}
 3 sensitivity in the whole f_s range of 1 - 99%, b) average α_{abs} sensitivity in three f_s ranges, and (c) average
 4 BB(%) sensitivities in three f_s ranges.

5

6



1



2

3 Figure 8. Bimodal particle size distributions with size-independent shell volume fractions f_s in two
 4 modes as a function of geometric mean diameters of mode 1 ($D_{g,1}$) and mode 2 ($D_{g,2}$). a) absorption
 5 Ångström exponent (α_{abs}) and the from it calculated fraction of biomass-burning BC (BB(%)) with the
 6 Aethalometer model constants of b) $\alpha_{ff} = 1$, $\alpha_{bb} = 2$ and c) $\alpha_{ff} = 0.9$, $\alpha_{bb} = 1.68$. The widths, the relative
 7 number of particles in the two modes and the shell volume fractions of the two modes on the left
 8 column: $\sigma_{g1} = 1.6$, $\sigma_{g2} = 1.6$, $N_1 = N_2$, $f_{s1} = 50\%$, $f_{s2} = 98\%$ and on the right column: $\sigma_{g1} = 1.4$, $\sigma_{g2} = 1.6$, N_1
 9 $= 10N_2$, $f_{s1} = 5\%$, $f_{s2} = 98\%$.